Aerial Manipulator Suspended from a Cable-Driven Parallel Robot: Preliminary Experimental Results

Arda Yigit, Miguel Arpa Perozo, Mandela Ouafo, Loïc Cuvillon, Sylvain Durand, Jacques Gangloff

Aerial Manipulator Suspended from a Cable-Driven Parallel Robot: Preliminary Experimental Results

Arda Yiğit, Miguel Arpa Perozo, Mandela Ouafo, Loïc Cuvillon, Sylvain Durand and Jacques Gangloff

Abstract— **Since omnidirectional aerial vehicles can generate a six degrees of freedom wrench, they could be used for dexterous manipulation tasks without the need for an additional robotic arm. However, they suffer from a reduced efficiency and dynamics range due to the huge amount of energy lost in gravity compensation.**

In this work, we introduce an omnidirectional aerial manipulator suspended from a cable-driven parallel robot (CDPR) by a spring, combining the advantages of the CDPR large workspace with the high dynamics of aerial vehicles, while reducing energy consumption thanks to gravity compensation.

A partitioned control scheme is implemented to regulate both systems separately. A preliminary control strategy is proposed for the CDPR motion that minimizes the total energy consumption. Experiments are carried out to assess the added value of the CDPR carrier.

I. Introduction

Some classes of robotic manipulator are particularly lightweight with respect to the size of their workspace. Aerial manipulators and cable-driven parallel robots (CDPR) belong to these classes and could be qualified as "frugal" with respect to manufacturing energy and raw material requirements. Indeed, some commercially available CDPRs like the Skycam or the Spidercam [https://www.spidercam.tv] may cover large areas of up to 250m x 250m using only four winches as actuators. Rotations might also be controlled by cables like with the eight-cable suspended CDPR CoGiRo [1] that covers a 16m x 12m x 6m workspace, but orientations might as well be handled by a more conventional robot mounted on the CDPR platform without increasing too much the complexity of the system [2]. Aerial manipulators are using propulsion units based on the reaction force produced by air acceleration, usually with propellers driven by electric motors. Various configurations are possible [3]. Simple tasks such as pick and place can be performed using flying hands, where a gripper is attached to an unmanned aerial vehicle (UAV). For tasks requiring more dexterity, the aerial vehicle is often equipped with one or more robotic arms. With an omnidirectional aerial vehicle, it is possible to achieve dexterous tasks without using an additional manipulator, thus simplifying the mechanical structure and improving the frugality of the design. These vehicles can either use non-steerable thrusters (e.g. the omnidirectional multirotor vehicle from Brescianini and D'Andrea [4] or the ODAR from Park et al. [5]) or steerable thrusters (e.g. the FAST-Hex from Ryll et al. [6] or the OMAV from Brunner et al. [7]). Without steering mechanism, the vehicle usually needs more thrusters to achieve the same controllability, but with a cheaper mechanical design. While six bidirectional non-steerable thrusters are sufficient to control all six degrees of freedom (DoFs), a redundant design with at least seven thrusters is needed when using unidirectional thrusters [8].

In [4] Brescianini and D'Andrea developed an omnidirectional multirotor vehicle actuated by eight nonparallel bidirectional thrusters. They are positioned in an optimal configuration maximizing the agility, i.e. the highest thrust and torque that can be generated in all directions, while enforcing rotational invariance. Nonlinearities are canceled with a feedback linearization approach. A control allocation computes the rotor velocity input signal by minimizing the power consumption while limiting the difference between the desired thrust and the actual thrust. An external tachometer is used to accurately regulate the propeller velocity. The ODAR [5] which is designed for omnidirectional aerial wrench generation also uses eight nonparallel bidirectional thrusters that are positioned to maximize the minimum-guaranteed omnidirectional wrench. The OMAV [7] uses only six pairs of steerable coaxial propellers for actuation. Nonlinear model predictive control is used to compute the desired wrench while taking into account the physical limitations of the system.

Aerial manipulators consume a lot of energy to compensate for gravity when they are static. This drastically reduces their autonomy when running on batteries. With a tether [9], the autonomy may theoretically be infinite but at the cost of some limitations in the workspace. CDPRs usually have a smaller workspace that non-tethered aerial manipulators due to limited cable length. Suspended CDPRs also consume some energy to carry the platform and fully-constrained CDPRs might even consume more energy to maintain some desired tension in the cables (e.g. to increase the stiffness of the platform). But for a given static payload, aerial manipulators consume far more energy to compensate for the gravity than CDPRs. Indeed, on a CDPR, when the platform is static, no mechanical energy is consumed, only electrical energy, mainly in the motor windings due to resistive losses. While on an aerial manipulator, since the propellers rotate at high speed to generate a thrust, the required mechanical power of the motor is high and resistive losses are still significant.

The suspension of the aerial vehicle reduces drastically en-

This work was supported by the e-VISER project funded by the French National Research Agency (ANR-17-CE33-0008).

The authors are with the ICube Laboratory, University of Strasbourg, INSA Strasbourg, 67000, Strasbourg, France (e-mail: arda.yigit@unistra.fr; miguel.arpaperozo@etu.unistra.fr; ouafomandela@gmail.com; l.cuvillon@unistra.fr; sylvain.durand@insa-strasbourg.fr; jacques.gangloff@unistra.fr).

ergy consumption thanks to gravity compensation. The cable-suspended aerial manipulator SAM [10] is an example of an omnidirectional aerial manipulator suspended by winch-actuated cables that carries a 7DoF serial manipulator. On the SAM, the platform holding the thrusters is the end effector of a suspended CDPR since actuated winches may help control the platform orientation. The architecture of this CDPR is original since all the cables share a unique anchoring point. Similar concepts combining aerial manipulator and CDPR exist in various fields. El Ghazaly et al. uses cables to actuate an underwater manipulator, increasing its lifting capabilities [11]. Erskine et al. [12] uses three quadrotor drones to tow a single platform using cables. Though this system has no gravity compensation, it also mixes cable-driven parallel actuation and aerial actuation.

In a previous project at our lab, we equipped a planar CDPR with cold air thrusters [13] and propellers [14], mainly to improve its dynamics. Then, with the Aerial Manipulator with Elastic Suspension (AMES) [15], we extended this concept to 6DoF and simplified the mechanical design using only a single spring to compensate for the gravity. With this architecture, there is only one compliant link, coupling an omnidirectional UAV to a robotic carrier. A low-stiffness spring, replacing the cable+winch subsystem of the SAM, provides both mechanical simplicity and reduced energy consumption by compensating for the gravity. Furthermore, the spring decouples the aerial vehicle from its carrier, so its motion is not limited anymore by the dynamics of the carrier. Experimental results showed that the AMES is able to achieve millimetric accuracy and fast dynamics without a carrier. A computed torque control law was proposed and its stability was proven using singular perturbation theory.

In this work, we add a four-cable suspended CDPR carrier to the AMES. Indeed, without a carrier, the workspace of the aerial manipulator is restricted around its equilibrium point due to the spring restoring force. Furthermore, this restoring force yields additional energy consumption for trajectories staying a long time away from the equilibrium point. However, if the equilibrium point could move along with the aerial manipulator, even at a slower pace, energy consumption could be significantly reduced and the workspace of the AMES could match the workspace of the CDPR. Indeed, the motion of the equilibrium point would not hinder the dynamics of the AMES thanks to the decoupling action of the spring. This is the main idea of this work. To our best knowledge, such a system has not yet been proposed nor studied from an energy consumption perspective.

The proposed system is first described in section II. Then the models of the CDPR and aerial manipulator dynamics are derived in section III. A partitioned control law is proposed in section IV and experimental results comparing energy consumption for test trajectories are given in section V.

II. Robot Description

We designed and implemented the robot shown in Fig. 1, where an omnidirectional aerial manipulator is suspended from the platform of a four-cable CDPR by a spring.

The aerial manipulator, which is called hereafter an Aerial Wrench Generator (AWG), was described in detail in a previous paper [15]. It has the same structure as an omnidirectional multirotor vehicle described in [4] and can generate a 6DoF wrench thanks to six bidirectional propulsion units or thrusters. The relative placement of propulsion units is optimized to maximize the agility, i.e. the highest thrust and torque that can be generated in all directions. Each propulsion unit (see Fig. 1) is made of a pair of propellers (DALPROP 5045), mounted on two coaxial brushless DC motors (T-Motor F-40 Pro III Kv2400), in order to be able to generate a force in both directions without changing direction of rotation. According to the sign of the force to be generated, the corresponding propeller rotates at the desired speed while the second one is idling, i.e. rotating at its lowest speed ($1500\,\mathrm{rpm}$, equivalent to $0.03\,\mathrm{N}$). To drive the rotational speed of the propellers, we developed the open-source Teensyshot firmware (https://github.com/jacqu/teensyshot) that implements a fast PID (proportional-integral-derivative) speed regulation loop on Teensy 4.0 development boards using real-time telemetry data acquired from KISS 32A electronic speed controllers (ESCs).

The spring compensates for the gravity, so the AWG is almost freely floating around its equilibrium position, and is therefore very energy efficient. For large displacements, the CDPR is used to slowly move the equilibrium point of the AWG to the average position of the current task in order to further reduce the energy consumption.

This AMES combines the large workspace capabilities of CDPRs and the high dynamics of UAVs while avoiding their autonomy limitations. The spring is decoupling the CDPR motion from the AWG motion. The sole purpose of the CDPR is to slowly translate the equilibrium point, thus a limited number of cables are required (a minimum of three), since the rotations are exclusively handled by the AWG.

The AWG is autonomous: it carries its own energy source, a $2300\,\mathrm{mA\,h}$, $11.1\,\mathrm{V}$ / 3S lithium polymer battery pack (TATTU 3S1P). It also has an on-board CPU (Raspberry Pi 4B) running high-level control algorithms and communicating with other remote devices through Wi-Fi TCP/IP sockets thanks to the open-source Simulink toolbox RPIt developed in our lab [16].

The CDPR carrier is a commercial product provided by Haption called Inca™, [https://www.haption.com/en/products-en/inca-en.html].
The anchoring point of the spring is driven by four cables. Each cable is equipped with a balancing spring to maintain tension in the cable and also to create a passive equilibrium point, reducing the energy consumption even more. The CDPR is actuated by four Maxon RE40 (48V) DC motors with encoders. Each motor drives two winches with helical grooves, one for the spring side and the other one for the end-effector side. A digital PI (proportional-integral) controller running on an FPGA regulates the current of each motor at $25\,\mathrm{kHz}$. The higher-level controller runs on the on-board CPU of the AWG and handles the digital

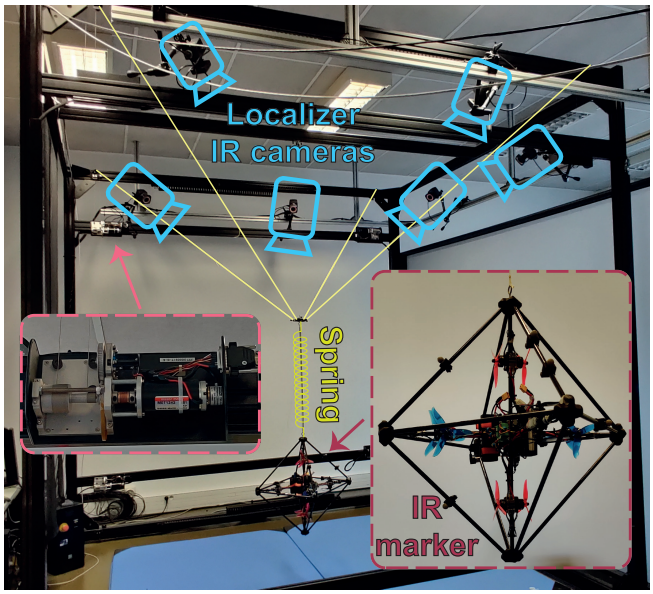

Fig. 1. Experimental setup.

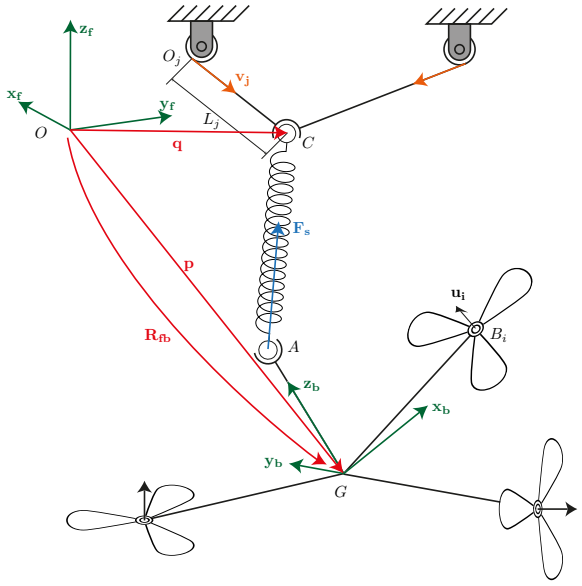

Fig. 2. AMES parameters

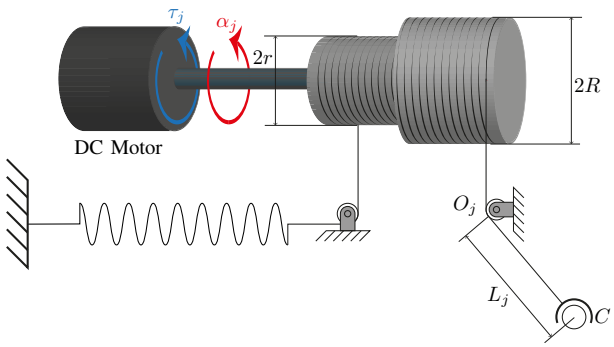

Fig. 3. CDPR actuated winch parameters

regulation of the cable winches angular velocity, the position control of the anchoring point (translations) and the pose control of the AWG (translations and rotations). These control loops are using respectively feedbacks from the winch motor encoders, the 3D measurements of a Vicon Bonita motion-capture system (infrared markers on the anchoring point and on the AWG) and from an on-board IMU (MPU-9150).

III. Modeling

A. Parametrization and Notations

The geometric parameters of the system are shown in Fig. 2 and Fig. 3.

Let $\mathcal{R}_f = (O, \mathbf{x_f}, \mathbf{y_f}, \mathbf{z_f})$ be an inertial frame with O its origin and $\mathcal{R}_b = (G, \mathbf{x_b}, \mathbf{y_b}, \mathbf{z_b})$ a moving frame positioned at the center of mass (CoM) G of the AWG with its $\mathbf{z_b}$ axis pointing toward the on-board anchoring point of the spring A. The rotation matrix $\mathbf{R_{fb}} \in SO(3)$ describes the orientation of $\mathcal{R}_b$ with respect to $\mathcal{R}_f$. The AWG has six propulsion units. The position of the center of the i-th propulsion unit is B_i, and $\mathbf{u_i}$ is the unit thrust direction vector. The CDPR has four cables which intersection is the second anchoring point of the spring C. The position vectors of the CoM G and of the cable intersection C are respectively $\mathbf{p}$ and $\mathbf{q}$. Thanks to a tiny deflection pulley, the cable output position O_j at the winch side is considered constant, with $\mathbf{v_j}$ the unit direction vector such that $\mathbf{O_jC} = L_j\mathbf{v_j}$ where $L_j \geq 0$ is the length of the j-th cable. The force applied by the spring on the AWG is noted $\mathbf{F_s}$. The spring force is the only coupling between the AWG and the CDPR dynamics and it can be expressed as:

$$\mathbf{F_s} = k\left(\|\mathbf{AC}\| - l_0\right)\frac{\mathbf{AC}}{\|\mathbf{AC}\|}$$

with l_0 the free length and k the stiffness of the spring.

The angular position of the j-th motor is α_j. The motor exerts a torque τ_j on the winch. The radii of the winches are r and R respectively for the balancing-spring side and the end-effector side.

Let $\mathbf{u}$ and $\mathbf{v}$ be vectors and $\mathcal{R}_q$ a reference frame. The projection of $\mathbf{v}$ in $\mathcal{R}_q$ is written ${}^q\mathbf{v}$. The cross product of ${}^q\mathbf{u}$ and ${}^q\mathbf{v}$ is denoted ${}^q\mathbf{u} \times {}^q\mathbf{v}$ and $[\cdot]_\times$ is the cross product matrix such that ${}^q\mathbf{u} \times {}^q\mathbf{v} = [{}^q\mathbf{u}]_\times {}^q\mathbf{v}$.

To simplify the notations, since the position vectors $\mathbf{p}$ and $\mathbf{q}$ are always expressed in the inertial frame $\mathcal{R}_f$, we omit the subscript: $\mathbf{p} = {}^f\mathbf{p}$ and $\mathbf{q} = {}^f\mathbf{q}$.

B. AWG Dynamics

Let $\mathbf{X} = (\mathbf{p}^T\ \boldsymbol{\eta}^T)^T$ be the pose coordinates of the AWG, with $\boldsymbol{\eta}$ a set of Euler angles. The dynamic model of the AWG is developed in [15] and is given as follows in the Cartesian-space canonical formulation:

$$\mathbf{M_a}(\mathbf{X})\ddot{\mathbf{X}} + \mathbf{C_a}(\mathbf{X}, \dot{\mathbf{X}})\dot{\mathbf{X}} + \mathbf{G_a}(\mathbf{X}, \mathbf{q}) = \tilde{\mathbf{W}}(\mathbf{X})\mathbf{w_2} \quad (1)$$

with

$$\begin{cases} \mathbf{M_a}(\mathbf{X}) &= \begin{pmatrix} m\mathbf{I}_3 & \mathbf{0}_3 \\ \mathbf{0}_3 & \mathbf{S}^T {}^b\mathbf{I_a}\mathbf{S} \end{pmatrix} \\ \mathbf{C_a}(\mathbf{X}, \dot{\mathbf{X}}) &= \begin{pmatrix} \mathbf{0}_3 & \mathbf{0}_3 \\ \mathbf{0}_3 & \mathbf{S}^T({}^b\mathbf{I_a}\dot{\mathbf{S}} + [\mathbf{S}\dot{\boldsymbol{\eta}}]_\times {}^b\mathbf{I_a}\mathbf{S}) \end{pmatrix} \\ \mathbf{G_a}(\mathbf{X}, \mathbf{q}) &= \begin{pmatrix} -m{}^f\mathbf{g} - {}^f\mathbf{F_s} \\ -\mathbf{S}^T {}^b\mathbf{N^s} \end{pmatrix} \\ \tilde{\mathbf{W}}(\mathbf{X}) &= \begin{pmatrix} \mathbf{R_{fb}} & \mathbf{0}_3 \\ \mathbf{0}_3 & \mathbf{S}^T \end{pmatrix} \mathbf{W}_b \end{cases}$$

where $m > 0$ is the total mass of the platform, ${}^b\mathbf{I_a} \in \mathbb{R}^{3\times3}$ its inertia tensor at the CoM expressed in $\mathcal{R}_b$, ${}^f\mathbf{g} \in \mathbb{R}^3$ the gravity acceleration, ${}^f\mathbf{F_s} \in \mathbb{R}^3$ the force of the elastic link on the AWG and ${}^b\mathbf{N^s} \in \mathbb{R}^3$ the associated torque at the CoM. The matrix $\mathbf{S}(\boldsymbol{\eta}) \in \mathbb{R}^{3\times3}$ is the analytical Jacobian, mapping the time derivative of $\boldsymbol{\eta}$ to the angular velocity. The matrix $\mathbf{W}_b \in \mathbb{R}^{6\times6}$ maps the column matrix $\mathbf{w}_2 = (\cdots \ w_i|w_i| \ \cdots)^T$ of signed squared propeller rotational velocities w_i to the wrench they apply on the platform expressed in the body frame $\mathcal{R}_b$.

C. CDPR Dynamics

We assume that the CDPR platform (i.e. at the intersection of the four cables) is massless. Indeed, since only the translational motion is required for the CDPR, the platform might be very small, almost punctual. Furthermore, it is manufactured using 3D printing with an ABS filament. This explains why the mass of this small and light part can be neglected. The cables are considered as straight lines and their elasticity is neglected compared to the elasticity of the balancing springs.

With these assumptions, the dynamic model of the CDPR in its canonical form becomes [17], [18]:

$$\mathbf{M_c}(\mathbf{q})\ddot{\mathbf{q}} + \mathbf{C_c}(\mathbf{q}, \dot{\mathbf{q}})\dot{\mathbf{q}} + \mathbf{G_c}(\mathbf{q}, \mathbf{p}) = -\mathbf{J}^T\boldsymbol{\tau} \qquad (2)$$

with

$$\begin{cases} \mathbf{M_c}(\mathbf{q}) &= \frac{1}{R}\mathbf{J}^T\mathbf{I_c}\mathbf{J} \\ \mathbf{C_c}(\mathbf{q}, \dot{\mathbf{q}}) &= \frac{1}{R}\mathbf{J}^T\mathbf{I_c}\dot{\mathbf{J}} \\ \mathbf{G_c}(\mathbf{q}, \mathbf{p}) &= k_c\frac{r^2}{R}\mathbf{J}^T(\mathbf{L} - \mathbf{L_0}) - R{}^f\mathbf{F_s} \end{cases}$$

where k_c is the balancing-spring stiffness, $\mathbf{I_c} \in \mathbb{R}^{4\times4}$ the diagonal matrix of actuator inertiae, $\boldsymbol{\tau} \in \mathbb{R}^4$ the motor torques, $\mathbf{L_0} \in \mathbb{R}^4$ the cable lengths at the equilibrium of the unforced system ($\mathbf{w_2} = \mathbf{0}$), $\mathbf{J} \in \mathbb{R}^{4\times3}$ the Jacobian matrix of the CDPR relating the anchoring point velocity $\dot{\mathbf{q}}$ to $\dot{\mathbf{L}}$, that is the time derivative of the (varying) cable lengths $\mathbf{L} \in \mathbb{R}^4$.

IV. Control

We propose a partitioned control scheme to impose a desired trajectory $\mathbf{X_{ref}} = ({\mathbf{p_{ref}}}^T \ {\boldsymbol{\eta}_{\mathbf{ref}}}^T)^T$ on the end effector, or equivalently on the AWG CoM (see Fig. 4). This choice is relevant thanks to the spring decoupling the dynamics of both subsystems: the AWG and the CDPR dynamics depend only on the relative positions of the spring ends A and C. Furthermore, independently from this decoupling, the CDPR is supposed to be much slower than the AWG (15 times slower with our experimental setup). So the pose control loop of the AWG will be tuned to track small displacements with high accelerations while the CDPR position loop will be responsible for large amplitude and slow acceleration motion tracking.

A. Redundancy Handling

We introduce here a simple solution to deal with the actuator redundancy that reduces the energy consumption. In a previous work, we showed that the energy consumption of the AWG increases significantly with the torque $\mathbf{N_s}$ generated by the spring restoring force on the AWG [15]. Therefore, the anchoring point reference position $\mathbf{q_{ref}}$ is chosen such that the AWG CoM G and the spring ends A and C stay aligned with constant relative distances:

$$\mathbf{q_{ref}} = \mathbf{p_{ref}} + \mathbf{R_{fb}}(\boldsymbol{\eta}_{\mathbf{ref}}) \begin{pmatrix} 0 \\ 0 \\ \delta z_{eq} \end{pmatrix}$$

with $\mathbf{R_{fb}}(\boldsymbol{\eta}_{\mathbf{ref}})$ the rotation matrix $\mathbf{R_{fb}}$ at orientation $\boldsymbol{\eta}_{\mathbf{ref}}$ and δz_{eq} the vertical distance between G and C at equilibrium of the unforced system.

In particular, with this strategy, if the reference trajectory is at constant orientation, the anchoring point just follows the movement of the AWG with an offset. Furthermore, if the reference orientation corresponds to vector $\mathbf{GA}$ being vertical, the control scheme will tend to maintain the spring anchoring point C on the vertical line going through G and maintain a constant distance $\|CG\|$.

Note that finding the optimal $\mathbf{q_{ref}}$ that minimizes the AWG energy consumption consists in minimizing $\|\mathbf{w_2}\|_{\frac{3}{2}}$, with $\|\cdot\|_{\frac{3}{2}}$ the $\frac{3}{2}$-norm, since the power consumption of a propulsion unit is affine with respect to the cubic rotational velocity [15]. In steady state, since $\tilde{\mathbf{W}}(\mathbf{X})^{-1}\mathbf{G_a}(\mathbf{X}, \mathbf{q}) = \mathbf{w_2}$, this can be written as a nonlinear optimization problem:

$$\mathbf{q_{ref}} = \min_{\mathbf{q}} \left\| \tilde{\mathbf{W}}(\mathbf{X})^{-1}\mathbf{G_a}(\mathbf{X}, \mathbf{q}) \right\|_{\frac{3}{2}}$$

B. AWG Control

The AWG follows a desired trajectory $\mathbf{X_{ref}}$ using a computed torque controller running at $100\,\mathrm{Hz}$ in the form

$$\tilde{\mathbf{W}}\mathbf{w}_2 = \mathbf{M_a}(\ddot{\mathbf{X}}_{\mathbf{ref}} + \mathbf{u}) + \mathbf{C_a}\dot{\mathbf{X}} + \mathbf{G_a} \qquad (3)$$

with $\mathbf{u}$ a feedback control input.

Computed torque control consists in inverting the dynamics of a system in order to obtain linear error dynamics. A linear control strategy can then be applied to the resulting error dynamics.

Here, we use a PID controller: $\mathbf{u} = \mathbf{K_p}(\mathbf{X_{ref}} - \mathbf{X}) + \mathbf{K_d}(\dot{\mathbf{X}}_{\mathbf{ref}} - \dot{\mathbf{X}}) + \mathbf{K_i}\int(\mathbf{X_{ref}} - \mathbf{X})$. The stability of a computed torque control for the AWG with a static anchoring point has been discussed in [15].

C. CDPR Control

To reject significant nonlinearities due to dry friction on pulleys, a cascade control scheme is implemented (see Fig. 4) that runs at $400\,\mathrm{Hz}$.

The inner loop consists in a PI controller regulating the rotational velocity $\dot{\boldsymbol{\alpha}}$ of the winches.

The outer loop that tracks the translational position reference $\mathbf{q_{ref}}$ implements a proportional controller with a feedforward term (P+ff):

$$\dot{\boldsymbol{\alpha}}_{\mathbf{ref}} = \frac{1}{R}\mathbf{J}\left(k_{ff}\dot{\mathbf{q}}_{\mathbf{ref}} + k_q(\mathbf{q_{ref}} - \mathbf{q})\right) \tag{4}$$

with k_{ff} and k_q positive gains and $\dot{\boldsymbol{\alpha}}_{\mathbf{ref}}$ the desired rotational velocity of the winches.

The exponential convergence toward $\mathbf{q_{ref}}$ of this control scheme using joint velocity inner loops has been first proven in [19] for serial robots. Since then, this two-loop cascade control scheme has been successfully applied to redundant robots [20], parallel robots [21] and CDPRs [22].

To guarantee positive tension of the cables, a tension distribution algorithm can be included if required [22]. However, with the present suspended configuration and the balancing springs that guarantee a minimal tension, all the cable tensions remained positive during the experiments.

V. Results

The performance of the AMES is assessed experimentally. This section presents dynamic and energy performances of the robot. The reference paths used for the tests are obtained with a fifth-order polynomial trajectory generator. The experiments are available on the video associated to the paper [https://youtu.be/NxJjCoystsA].

A. Dynamic Maneuver Handling

A fast trajectory reference is used to highlight the heterogeneous dynamics of the AMES as shown in Fig. 5, where $\delta\mathbf{p}$ and $\delta\mathbf{q}$ are the relative positions of the AWG and the anchoring point with respect to their initial position. As expected, the AWG follows with millimetric precision the reference trajectory while the CDPR anchoring point lags behind during transients. The platform behaves in closed loop as a first-order system with $0.5\,\mathrm{s}$ time constant after controller tuning. It can also be noted that the steady-state error tends toward zero for both responses.

B. Energy Consumption

Two experiments are carried out to assess the added value of the CDPR carrier with respect to energy consumption. First, the same AWG trajectory $\mathbf{X_{ref}}$ with a vertical $\boldsymbol{\eta}_{\mathbf{ref}}$ is tracked with and without motion of the CDPR.

The ESCs provide in real time battery voltage U and current i_e. So it is possible to obtain the electrical power delivered to an ESC: $P_e = Ui_e$.

The power consumption of the CDPR can be estimated by adding the mechanical power output and the resistive losses, neglecting core losses and switching losses in the winch drive MOSFETs. The mechanical power output of a motor is the product of the torque τ_j by the rotational velocity $\dot{\alpha}_j$. Since the torque is proportional to the current i_c, the mechanical power becomes: $P_m = k_{em}i_c\dot{\alpha}$, with k_{em} the torque constant of the motor. Knowing the resistance of the windings R_m, the resistive losses are: $P_c = R_m i_c^2$. Hence, the estimated power consumption of a motor is given by: $P_{motor} = k_{em}i_c\dot{\alpha} + R_m i_c^2$.

The relative positions of the AWG and of the CDPR carrier, as well as the power consumption of the propulsion units, are given in Fig. 6. It is worth noticing that the carrier does not have a significant impact on the root-mean-square error (RMSE) of the AWG position (see Table I): the RSME stays submillimetric as highlighted in [15]. Nonetheless, the power consumption of the propulsion units is clearly lower when the CDPR is used as a carrier, especially at steady state. This can be heard in the associated video: thanks to the carrier motion, the propeller noise tends to decrease at steady state. Without the carrier, the AWG consumes $3.27\,\mathrm{W\,h}$ during the trajectory. Adding the carrier lowers the consumption to $1.52\,\mathrm{W\,h}$ ($-52\,\%$). The global energy consumption is also significantly reduced since the carrier only consumes $0.05\,\mathrm{W\,h}$.

The carrier also improves energy efficiency for orientations. For a $5\,\mathrm{deg}$ roll angle, the average power consumption with the carrier is $92.5\,\mathrm{W}$, $-51\,\%$ less than without the carrier ($188.6\,\mathrm{W}$).

Axis	$\mathbf{x_f}$	$\mathbf{y_f}$	$\mathbf{z_f}$
With carrier	0.56	0.61	0.34
Without carrier	0.45	0.39	0.42

TABLE I
RMSE PER AXIS IN [mm].

VI. Conclusion and Future Work

In this paper, we present an omnidirectional aerial manipulator suspended from a cable-driven parallel robot (CDPR) by a spring. The aerial manipulator allows for high dynamics and the CDPR for large displacements while improving energy efficiency. A partitioned controller is implemented to regulate separately the aerial manipulator pose with a computed torque controller and the CDPR position with a kinematic cascade controller. A simple strategy is used to determine the desired position of the CDPR platform from the reference pose of the AWG to reduce energy consumption.

We show that with the proposed strategy, the CDPR carrier can reduce by half the energy consumption of the system while maintaining the millimetric accuracy of the aerial manipulator.

A nonlinear optimization problem that could be solved offline is suggested to find the optimal trajectory of the CDPR platform minimizing energy consumption.

Future research should consider nonlinear model predictive control to allocate the control simultaneously for both the aerial manipulator and the CDPR with respect to their dynamics, while minimizing in real time the energy consumption.

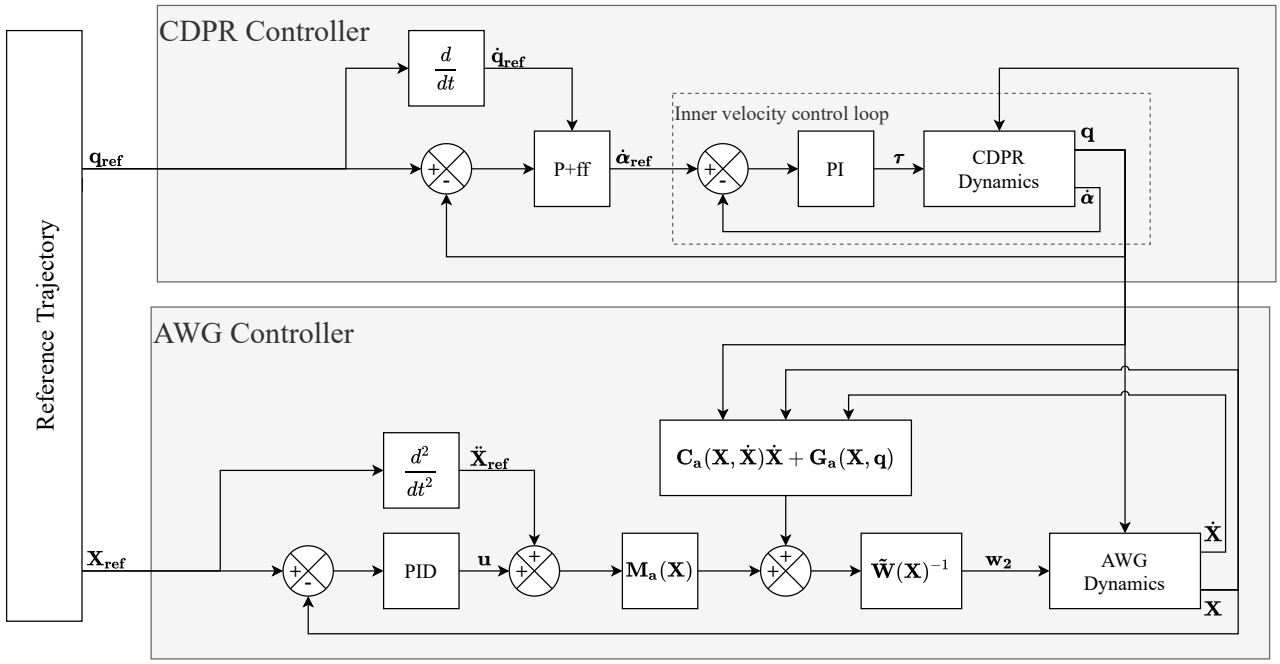

Fig. 4. AMES controller.

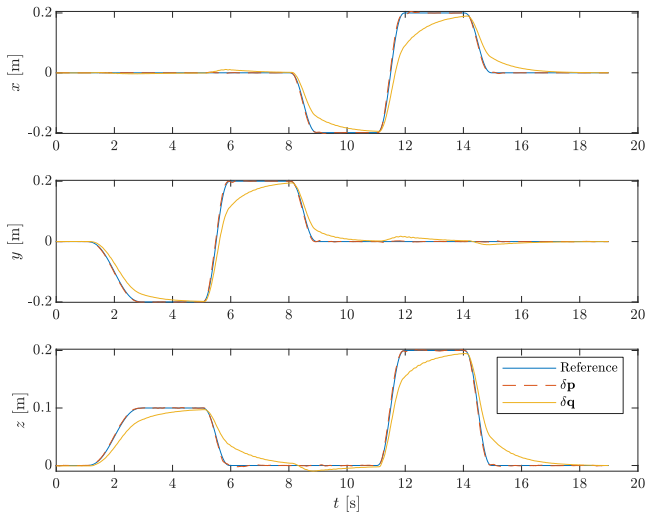

Fig. 5. AWG dynamic maneuvers.

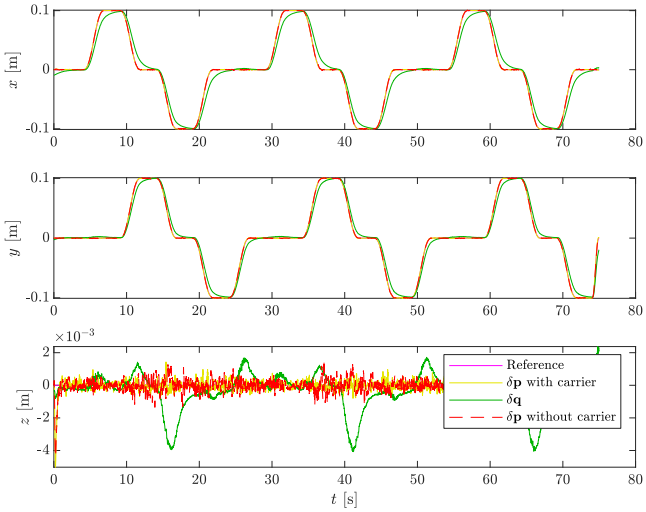

(a) Trajectories.

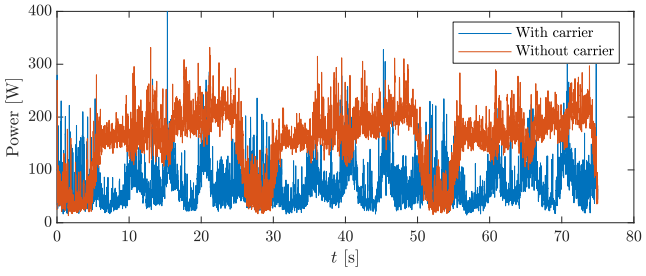

(b) Power consumption.

Fig. 6. AWG power consumption comparison with and without the CDPR carrier.

References

[1] M. Gouttefarde, J. Collard, N. Riehl, and C. Baradat, "Geometry selection of a redundantly actuated cable-suspended parallel robot," *IEEE Transactions on Robotics*, vol. 31, no. 2, pp. 501–510, 2015.

[2] D. Bury, J. Izard, M. Gouttefarde, and F. Lamiraux, "Continuous collision detection for a robotic arm mounted on a cable-driven parallel robot," in *2019 IEEE/RSJ International Conference on Intelligent Robots and Systems (IROS)*, 2019, pp. 8097–8102.

[3] F. Ruggiero, V. Lippiello, and A. Ollero, "Aerial Manipulation: A Literature Review," *IEEE Robotics and Automation Letters*, vol. 3, no. 3, pp. 1957–1964, 7 2018. [Online]. Available: https://ieeexplore.ieee.org/document/8299552/

[4] D. Brescianini and R. D'Andrea, "An omni-directional multirotor vehicle," *Mechatronics*, vol. 55, pp. 76–93, 11 2018. [Online]. Available: https://linkinghub.elsevier.com/retrieve/pii/S0957415818301314

[5] S. Park, J. Lee, J. Ahn, M. Kim, J. Her, G.-H. Yang, and D. Lee, "ODAR: Aerial Manipulation Platform Enabling Omnidirectional

Wrench Generation," *IEEE/ASME Transactions on Mechatronics*, vol. 23, no. 4, pp. 1907–1918, 8 2018. [Online]. Available: https://ieeexplore.ieee.org/document/8401328/

[6] M. Ryll, D. Bicego, and A. Franchi, "Modeling and control of FAST-Hex: A fully-actuated by synchronized-tilting hexarotor," in *2016 IEEE/RSJ International Conference on Intelligent Robots and Systems (IROS)*. IEEE, 10 2016, pp. 1689–1694. [Online]. Available: http://ieeexplore.ieee.org/document/7759271/

[7] M. Brunner, K. Bodie, M. Kamel, M. Pantic, W. Zhang, J. Nieto, and R. Siegwart, "Trajectory Tracking Nonlinear Model Predictive Control for an Overactuated MAV," in *2020 IEEE International Conference on Robotics and Automation (ICRA)*. IEEE, 5 2020, pp. 5342–5348. [Online]. Available: https://ieeexplore.ieee.org/document/9197005/

[8] M. Tognon and A. Franchi, "Omnidirectional Aerial Vehicles With Unidirectional Thrusters: Theory, Optimal Design, and Control," *IEEE Robotics and Automation Letters*, vol. 3, no. 3, pp. 2277–2282, 7 2018. [Online]. Available: http://ieeexplore.ieee.org/document/8281444/

[9] ——, *Theory and Applications for Control of Aerial Robots in Physical Interaction Through Tethers*, ser. Springer Tracts in Advanced Robotics. Cham: Springer International Publishing, 2021, vol. 140. [Online]. Available: http://link.springer.com/10.1007/978-3-030-48659-4

[10] Y. S. Sarkisov, M. J. Kim, D. Bicego, D. Tsetserukou, C. Ott, A. Franchi, and K. Kondak, "Development of SAM: cable-Suspended Aerial Manipulator *," in *2019 International Conference on Robotics and Automation (ICRA)*. IEEE, 5 2019, pp. 5323–5329. [Online]. Available: https://ieeexplore.ieee.org/document/8793592/

[11] G. El-Ghazaly, M. Gouttefarde, and V. Creuze, "Hybrid cable-thruster actuated underwater vehicle-manipulator systems: A study on force capabilities," in *2015 IEEE/RSJ International Conference on Intelligent Robots and Systems (IROS)*. IEEE, 9 2015, pp. 1672–1678. [Online]. Available: http://ieeexplore.ieee.org/document/7353592/

[12] J. Erskine, A. Chriette, and S. Caro, "Wrench Capability Analysis of Aerial Cable Towed Systems," in *Volume 5A: 42nd Mechanisms and Robotics Conference*. American Society of Mechanical Engineers, 8 2018. [Online]. Available: https://asmedigitalcollection.asme.org/IDETC-CIE/proceedings/IDETC-CIE2018/51807/QuebecCity,Quebec,Canada/275090

[13] H. Sellet, I. Khayour, L. Cuvillon, S. Durand, and J. Gangloff, "Active Damping of Parallel Robots Driven by Flexible Cables Using Cold-Gas Thrusters," in *2019 International Conference on Robotics and Automation (ICRA)*. IEEE, 5 2019, pp. 530–536. [Online]. Available: https://ieeexplore.ieee.org/document/8794061/

[14] I. Khayour, L. Cuvillon, C. Butin, A. Yiğit, S. Durand, and J. Gangloff, "Improving Disturbance Rejection and Dynamics of Cable Driven Parallel Robots with On-board Propellers," in *2020 IEEE/RSJ International Conference on Intelligent Robots and Systems (IROS)*. IEEE, 2020.

[15] A. Yigit, M. A. Perozo, L. Cuvillon, S. Durand, and J. Gangloff, "Novel Omnidirectional Aerial Manipulator With Elastic Suspension: Dynamic Control and Experimental Performance Assessment," *IEEE Robotics and Automation Letters*, vol. 6, no. 2, pp. 612–619, 4 2021. [Online]. Available: https://ieeexplore.ieee.org/document/9312497/

[16] J. Gangloff, A. Yiğit, and M. Lesellier, "RPIt," 2020. [Online]. Available: https://github.com/jacqu/RPIt/

[17] R. Chellal, L. Cuvillon, and E. Laroche, "Model identification and vision-based H_∞ position control of 6-DoF cable-driven parallel robots," *International Journal of Control*, vol. 90, no. 4, pp. 684–701, 2017. [Online]. Available: https://doi.org/10.1080/00207179.2016.1220623

[18] M. A. Khosravi and H. D. Taghirad, "Dynamic analysis and control of cable driven robots with elastic cables," *Transactions of the Canadian Society for Mechanical Engineering*, vol. 35, no. 4, pp. 543–557, 2011. [Online]. Available: https://doi.org/10.1139/tcsme-2011-0033

[19] R. Kelly and J. Moreno, "Manipulator motion control in operational space using joint velocity inner loops," *Automatica*, vol. 41, no. 8, pp. 1423–1432, 2005. [Online]. Available: https://www.sciencedirect.com/science/article/pii/S000510980500107X

[20] I. Soto and R. Campa, "Two-loop control of redundant manipulators: Analysis and experiments on a 3-dof planar arm," *International Journal of Advanced Robotic Systems*, vol. 10, no. 1, p. 85, 2013. [Online]. Available: https://doi.org/10.5772/53515

[21] R. Campa, J. Bernal, and I. Soto, "Kinematic modeling and control of the hexapod parallel robot," in *2016 American Control Conference (ACC)*, 2016, pp. 1203–1208.

[22] R. Chellal, L. Cuvillon, and E. Laroche, "A kinematic vision-based position control of a 6-dof cable-driven parallel robot," in *Cable-Driven Parallel Robots*, A. Pott and T. Bruckmann, Eds. Cham: Springer International Publishing, 2015, pp. 213–225.